Formation of sp^3-Bonded Carbon Nanostructures by Femtosecond Laser Excitation of Graphite

J. Kanasaki,[1] E. Inami,[1] K. Tanimura,[1,*] H. Ohnishi,[2] and K. Nasu[2]

[1]*The Institute of Scientific and Industrial Research, Osaka University, 8-1 Mihogaoka, Ibaraki, Osaka 567-0047, Japan*

[2]*Institute of Materials Structure Science, KEK, 1-1 Oho, Tsukuba, Ibaraki, 305-0801, Japan*

(Received 16 September 2008; published 23 February 2009)

A scanning tunneling microscopy study and *ab initio* total energy calculations have identified the atomic-level structure of novel sp^3-bonded carbon nanoscale domains formed dynamically from graphite by femtosecond-laser excitation. The structure is characterized by a pseudo sp^3-bonding configuration that results in inward displacement of surface carbon atoms by 0.5 Å in every third row along the $[1\bar{1}00]$ orientation. This structural periodicity is unique and differs from conventional phases of diamond.

DOI: 10.1103/PhysRevLett.102.087402 PACS numbers: 78.66.Tr, 61.80.Ba, 68.37.Ef, 73.20.At

Carbon exhibits various condensed phases composed of sp^3- and/or sp^2-bond orders [1–3]. Fundamental and technological interest in development of new carbon-based devices [4] has encouraged pursuit of new carbon phases with novel structural and electronic properties. Hexagonal graphite, characterized by an sp^2-bonded network, is the most stable crystalline solid phase at atmospheric pressure. Diamond, which consists of an sp^3-bonded network is the most stable phase under high pressure. Thermodynamic transformation between these two crystalline phases is possible only under high pressure [3]. However, a first-principles calculation suggests that a dynamical transformation path exists between graphite and diamond under electronic excitation [5]. Such an extreme nonequilibrium material-phase transformation is a promising avenue to form new condensed phases of matter [6].

A recent time-resolved electron diffraction study [7] has reported transient formation of an sp^3-like structure in graphite under intense fs-laser excitation below the melt threshold. Based on the diffraction-spectra analysis, they have shown that the transient structure has a 1.9 Å interlayer bond. However, direct atomic-level structural determination remains an important open question in laser-induced sp^3-like phase transformation of graphite. Here we report the direct atomic-scale identification of sp^3-like nanostructures dynamically formed from graphite by fs-laser excitation. Scanning tunneling microscopy (STM) and spectroscopy under ultrahigh vacuum (UHV) conditions have revealed nanoscale domains with a novel sp^3-bonded structure. We modeled the graphite sp^2 to sp^3-type bonding transformation using *ab initio* local density approximation calculations, and determined bonding and electronic properties in the nanodomains. The newly identified structure is not a conventional diamond structure, but has a novel sp^3-bonded configuration. This may be viewed as an intermediate and long-lived metastable phase between graphite and diamond.

Flat and clean surfaces of highly oriented pyrolytic graphite (HOPG) were prepared in a UHV chamber. Laser pulses with 80-fs temporal width, generated with a Ti:sapphire laser, were focused on samples placed on the stage of a UHV-STM at an incident angle of 45°. By combining a half-wave plate and a polarizer, the polarization and the intensities of fs-laser pulses were precisely controlled. Surface-atomic structures were imaged *in situ* at several sample-bias voltages (V_s) at room temperature.

Figure 1(a) shows a typical STM image (at $V_s = +100$ mV) acquired after exciting surfaces with 10^4 laser pulses at a fluence of 64 mJ cm^{-2}. Laser excitation generates domains with bright protrusions of typically a 5 nm diameter, which were completely absent prior to irradiation. In the domains, surface atoms are distorted from their original sites as described later, but no vacancies are generated. The number density N of such domains increases with the number of laser shots at a fixed intensity [8]. Therefore, fs-laser excitation induces structural changes on the graphite surface forming bright circular domains (BCDs) in STM images. BCDs thus formed survive more than a week when the irradiated surfaces are kept at room temperature in UHV.

The efficiency of domain formation is sensitive to excitation-laser characteristics. First, BCDs are produced only by fs-laser excitation. Excitation with ns-laser pulses (532 nm, 3 ns) did not form BCDs even at fluences greater than 190 mJ cm^{-2} where macroscopic damage occurred. Second, domain formation takes place specifically using p-polarized fs-laser light and the efficiency of formation depends superlinearly on excitation intensity. We determined the magnitude of N from a survey of more than 10^5 surface sites after 1×10^4 fs pulses at a fixed fluence. Excitation at fluences less than 60 mJ cm^{-2} did not induce any structural changes, even after 10^6 laser pulses. At fluences above 60 mJ cm^{-2}, however, N increased superlinearly with fluence, but only for p-polarized laser pulses. When the surfaces were excited with s-polarized light, no structural changes were induced even at fluences as high as 120 mJ cm^{-2}, above which macroscopic damage was generated on the surface. The excitation density n can be estimated using a rate equation model: $dn/dt = (1 - R) \times \alpha\phi(t) - (1/\tau)n$, where R is reflectivity, α the absorption

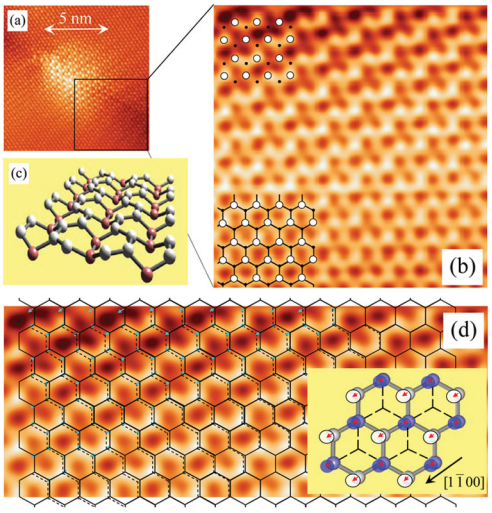

FIG. 1 (color). (a) A typical STM image of the HOPG surface acquired after excitation with 1×10^4 laser pulses, a fluence of 64 mJ cm^{-2}. The images were acquired with a Pt-Ir tip at a V_s of +100 mV. (b) The image acquired at a V_s of −40 mV for the region shown by a rectangle in (a) with an expanded scale. (c) A schematic model for the laser-altered configurations in the BCD. (d) Displacement of the center of each protrusion in the upper half of (b). The solid honeycomb lattice represents the original carbon-atom site on the pristine surface, while the dotted lattice is formed by combining the centers of observed protrusions.

coefficient, $\phi(t)$ the photon flux of a laser pulse, and τ the graphite carrier lifetime, respectively. For the maximum density $n_{\max}$, $dn/dt = 0$ at time $t = \tau_{\max}$, giving $n_{\max} = (1-R)\alpha\tau\phi(\tau_{\max})$. Using previous results of $\tau = 130$ fs and $\tau_{\max} \approx 50$ fs in Ref. [9], together with strong optical anisotropy of optical constants of graphite [10], $n_{\max}$ was 2.2×10^{22} cm^{-3} for p-polarized light at 64 mJ cm^{-2}, while it was 3.2×10^{22} cm^{-3} for s-polarized light at 120 mJ cm^{-2}. Therefore, the surface-structural changes are not simply governed by excitation density, but are specifically triggered by p-polarized light that has an electric vector component parallel to the c axis, showing the electronic origin of the transformation.

Because of the high brightness at the central part of a BCD, resolution is less reliable for atomic-scale structure analysis. Therefore, we analyze extensively the region shown by the rectangle in Fig. 1(a). Under typical conditions, only every other atom [referred to as visible (β) atoms hereafter], on the honeycomb graphite lattice is imaged by STM: primarily because of an electronic effect, specifically the small energy gap near the Fermi energy for the invisible (α) atoms with $2pz$ interaction [11]. This effect leads to a trigonal-symmetry image, as in the lower part of Fig. 1(a). Imaging of all surface atoms, including α atoms, is crucial for identifying atomic-level structures of the BCDs. We were able to image α atoms by carefully adjusting V_s. Figure 1(b) shows an STM image acquired at $V_s = -40$ mV for the region indicated by a rectangle in Fig. 1(a). The lower part of Fig. 1(b), which represents an unaltered region of the surface, shows the honeycomb-lattice arrangement from which we can identify α and β atoms unambiguously, as shown by dots and open circles, respectively, (invisible α atoms are weakly imaged).

The laser-altered domain region shows a different pattern. We plot the α and β atomic sites with dots and open circles with a small shift along the $[1\bar{1}00]$ direction extrapolated from a nonaltered region in the same image. It is evident that neighboring α and β atoms in each unit of the honeycomb lattice become dark, and form a trough along the $[1\bar{1}00]$ direction. Concurrently, the other pairs of α and β atoms in the same lattice form bright ellipses and zigzag dimer chains elongated parallel to the troughs. Instead of the electronic effects that distinguish atoms, new effects that induce changes in the local density of states (LDOS) govern the brightness of each surface atom within the domain region. If we simply interpret the changes in brightness as changes in the tip to atom distance, due to inward and outward displacement of the top-most carbon atoms, the structure schematically shown in Fig. 1(c) is predicted. This structure is totally different from that of the conventional cubic diamond when transferred from graphite via significant deformation of the unit cell; dark troughs due to intruded carbon atoms on the surface are formed along a $[\bar{1}\,\bar{1}\,20]$ direction for the cubic diamond [3]. On the other hand, if the up and down displacement along a $[1\bar{1}00]$ direction takes place alternatively, then the structure is just equivalent to the hexagonal diamond. However, the STM image shows a different periodicity; every third row becomes dark.

Modulations in STM images of graphite have often been ascribed to the electronic standing wave (ESW) effect due to scattering by surface defects [12]. Previous studies have shown that the ESW effect is commensurate with the underlying graphite lattice, and is independent of V_s, since the ESW effect results from large momentum scattering, characterized solely by the Fermi wavelength of $3a/2$ in the case of graphite because of its characteristic band structure (a is the lattice constant) [12]. Although such effects may be unavoidable to some extent, the observed features in Fig. 1 are not due to the ESW effect, but rather are due to structural changes on graphite surfaces. First, the images in Figs. 1(a) and 1(b), acquired at different V_s for the same region, show dramatic differences that cannot be explained by the ESW effect. Second, we show in Fig. 1(d) the displacement "map" of the atoms included in the domain. The shifts of the centers of all protrusions in the upper half of Fig. 1(b) were measured from their original graphite sites, and are indicated by arrows. It is clear that the center of each protrusion is systematically displaced depending on site; the maximum distortion is 0.3 Å. Therefore, the changes in the image are not commensurate with the graphite lattice. We conclude that the changes in the STM images in Fig. 1 are representative of laser-induced structural changes on the surface. Significantly, Fig. 2 shows that the atoms on the top-most plane exhibit a coherent shear displacement along $[1\bar{1}00]$. This provides a key piece of information for identification of the induced structure.

In order to stabilize the in-plane displacements displayed in Fig. 1(d), interlayer bonding is crucial. More definitive indication of the bonding is revealed by our observation that, under laser excitation, above 85 mJ cm^{-2}, intact sheet ablation, with a similar size of a few nm diameter, is induced *only* in the form of even-layer removal. Since HOPG has a stack sequence of *ABABAB*, the phase of atomic lines along the $[2\bar{1}\,\bar{1}\,0]$ one plane, representing the line connecting visible atoms, shifts spatially on each successive plane. STM-image analysis for the ablated regions shows clearly that a line along $[2\bar{1}\,\bar{1}\,0]$ on the top layer *always* shows the same alignment on the inner layer of the ablated region, without any exceptions. Therefore, an even number of graphene sheets (typically two) has been ablated under fs-laser excitation, indicating definitively that interlayer bonding is induced by fs-laser excitation of graphite.

To gain a deeper understanding of the photoinduced structural changes, we performed *ab initio* local density approximation total energy calculations of the adiabatic potentials germane to the structural transformations using a large-size cluster. We modeled two layers of graphene, with a Gaussian basis (STO-3G), each layer consisting of 200 carbon atoms, with dangling bonds in the *ab* plane terminated by H atoms. In general, close examination of domain formation of an appropriate size is crucial for establishing realistic transformation pathways and energetics, since structural phase transformations cannot take place in an entirely uniform fashion. In particular, we analyze here the formation of domains with a 5-nm diameter. To characterize a domain with an sp^2-graphite boundary structure, we introduced three modes of displacement as depicted in Fig. 2(a). Buckling, δ, represents the deviation from a sp^2-planer configuration to a sp^3-type configuration. Since HOPG has a stack sequence of *ABABAB*, β atoms on one plane do not have any bonding partner at the position just below them. Therefore, to establish a local sp^3-type bonded configuration, shear displacement, ΔQ, of the two layers is required. In fact, such a shear displacement has been confirmed in Fig. 1(d). Finally, the intrusion, Δz, of the center of a buckled plane from the original graphite plane, together with these distortions, characterizes the newly formed C-C bonds between two approaching layers and determines the laser-induced structures.

In Fig. 2(b), the calculated total energy for formation of the domain consisting of 128 atoms per layer is displayed as a function of the total intrusion ΔL $(=\Delta z + \delta/2)$ and ΔQ. We have the second minimum with an energy 0.69 eV/atom higher than the ground (graphite) state at $\Delta z = 0.65$ Å, $\delta = 0.5$ Å, and $\Delta Q = 0.25$ Å. The local configuration that gives the second minimum is shown in Fig. 2(c). Although STM measurements cannot determine ΔL and δ, the $\Delta Q = 0.25$ Å is close to that determined in Fig. 1(d). The top-down view of the calculated local structure is compared with the observed STM images in Fig. 2(d), where solid dots represent intruded C atoms and open circles represent extruded atoms. The calculated structure shows almost perfect agreement with the STM images of the laser-altered region. It is worth noting that the structure in Fig. 2(c) does not include any nonbonding $2pz$ states as in the cold-pressed graphite structure in Ref. [13]. The bonding configuration is similar to, though still significantly distorted from, the ideal sp^3 configuration. Even β atoms in the original graphite structure form a pseudo sp^3-like bonding via in-plane shear displacements, which contribute more than 30% of the energy stabilization as shown in Fig. 2(c). Therefore, the structure identified here is a novel sp^3-bonded carbon phase never reported previously. The stabilization energy of as much as 0.27 eV/atom means that this metastable configuration is quite stable at room temperature.

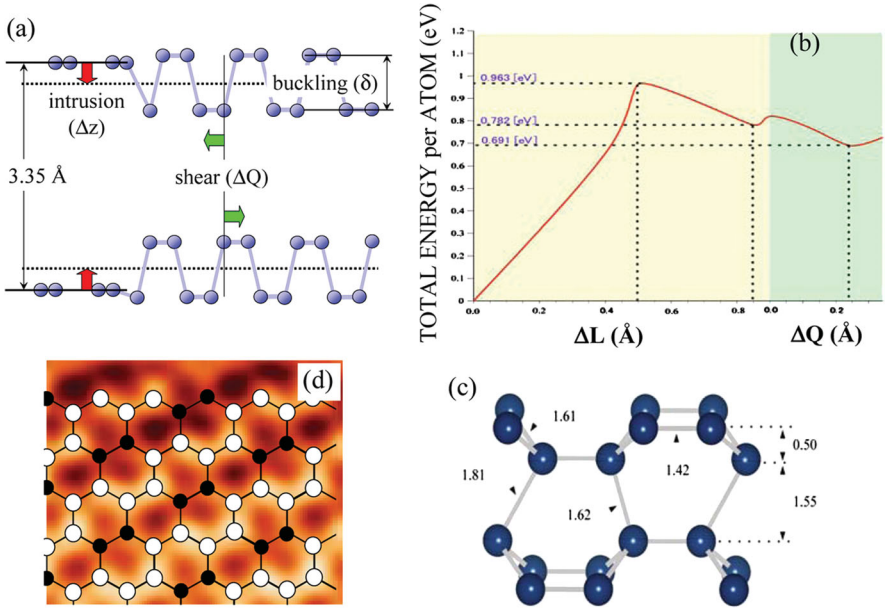

FIG. 2 (color). (a) Modes of displacements characterizing structural transformation from graphite to a sp^3-bonded domain. Buckling δ, shear displacement ΔQ, and intrusion Δz are defined in the figure. (b) Total energy of the adiabatic potential for formation of an sp^3-bonded structural domain as a function of the total intrusion $(\Delta L = \Delta z + \delta/2)$ and shear displacement ΔQ. (c) Local bonding structure in the domain forming the second minimum in (b). (d) Comparison between the STM image in Fig. 1(b) and the top-down view of the local structure of (c).

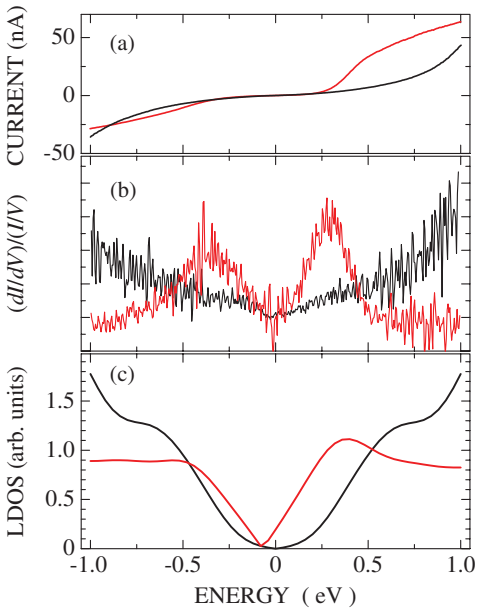

FIG. 3 (color). (a) I/Vcharacteristics of the tunneling injection for an unaltered graphite surface, black, and for a BCD, red. (b) The experimental LDOS for an unaltered graphite surface, black, and for a BCD, red. (c) Theoretical LDOS for graphite, black, and for the minimum configuration of the sp^3-bonded structural domain, red. The relative intensities are normalized with respect to the DOS in the region from -1 to 1 eV.

To further substantiate the correlation between the STM-image analysis and the theoretical results, we study the LDOS for a domain with sp^3-bonded structure. In Fig. 3(a), we show the I-V characteristics measured for a BCD and an unaltered region of the graphite surface. Significant differences are revealed. Based on the standard formula of scanning tunneling spectroscopy, the experimental LDOS are evaluated as LDOS $= (dI/dV)/(I/V)$ [14], and the results are shown in Fig. 3(b); the remarkable peak features at ± 0.3 V near the Fermi energy E_F ($E = 0$) are evident for the BCD. The theoretical results of LDOS for the sp^3-bonded domain and graphite are shown in Fig. 3(c), which also confirms qualitatively that the LDOS near E_F is enhanced for the sp^3-bonded domains, relative to the graphite surface. The enhancement results partly from the fact that the topological restriction that characterizes the linear increase of the LDOS near E_F for graphite is significantly relaxed for the sp^3-bonded configuration domain. LDOS peaks of both the occupied and unoccupied states near E_F result entirely from the incomplete sp^3-bonded configurations of the structure. We presume that the discrepancy between the experimental and theoretical LDOS spectra primarily results from the limited number of atoms used in the calculation, since the domain size changes the spectra significantly. Also, changes in characteristics of tunneling injection from graphite to the sp^3-bonded structure may induce possible differences between theoretical and experimental results. The domain-induced LDOS near the E_F makes it possible to image the spatial pattern of the newly formed sp^3 carbon structures by STM. Details of the calculations and theoretical aspects will be published separately [15].

As to the dynamics of forming this unique sp^3-bonded structure, it should be noted that both the interlayer compression and in-plane shear displacement are excited inherently under fs-laser excitation, as shown experimentally [7,16,17]. These coherent and dynamic nonlocal lattice motions may transiently distort local regions to make interlayer bond formation feasible. The specific role of the p-polarized light may be related to possible enhancement of such local distortions via interlayer charge transfer excitation that can only be induced by the electric vector component parallel to the c axis. The full elucidation of these dynamics is an interesting and important future problem pertaining to optical control of the new-phase formation in carbon.

In conclusion, we have identified the structure of sp^3-bonded carbon nanodomains formed by fs-laser excitation of graphite. The structure revealed here differs from thermodynamically formed conventional diamond, and may correspond to a new phase of carbon that can only be produced by nonequilibrium excitation of graphite with ultrashort laser pulses.

This work was supported by a specially promoted research of Grant-in-Aid for Scientific Research from the MEXT, Japan.

*tanimura@sanken.osaka-u.ac.jp

[1] H. W. Kroto *et al.*, Nature (London) **318**, 162 (1985).
[2] S. Iijima, Nature (London) **354**, 56 (1991).
[3] Y. Tateyama *et al.*, Phys. Rev. B **54**, 14 994 (1996).
[4] A. M. Stoneham, Nature Mater. **3**, 3 (2004).
[5] H. Nakayama and H. K. Yoshida, Jpn. J. Appl. Phys. **41**, L817 (2002).
[6] K. Yonemitsu and K. Nasu, Phys. Rep. **465**, 1 (2008).
[7] R. K. Raman *et al.*, Phys. Rev. Lett. **101**, 077401 (2008).
[8] The growth rate of number density of BCDs for the fluence of 64 mJ cm^{-2} is about 10^{-8} per nm^2 per pulse. Because of this small yield, we needed typically 10^4 laser pulses for characterization by means of STM. Consequently, we cannot say whether BCD formation requires many laser shots or is induced by a single shot with an appropriate intensity.
[9] K. Seibert *et al.*, Phys. Rev. B **42**, 2842 (1990).
[10] R. Ahuja *et al.*, Phys. Rev. B **55**, 4999 (1997).
[11] D. Tomanek *et al.*, Phys. Rev. B **35**, R7790 (1987).
[12] P. Ruffieux *et al.*, Phys. Rev. B **71**, 153403 (2005);
[13] W. L. Mao *et al.*, Science **302**, 425 (2003).
[14] J. A. Stroscio and R. M. Feenstra, in *Scanning Tunneling Microscopy*, edited by J. A. Stroscio and W. J. Kaiser (Academic, San Diego, 1993).
[15] H. Ohnishi and K. Nasu, Phys. Rev. B (to be published).
[16] T. Mishina, K. Nitta, and Y. Masumoto, Phys. Rev. B **62**, 2908 (2000).
[17] F. Carbone *et al.*, Phys. Rev. Lett. **100**, 035501 (2008).